JACS
JOURNAL OF THE AMERICAN CHEMICAL SOCIETY
Article
pubs.acs.org/JACS

Why Are Diphenylalanine-Based Peptide Nanostructures so Rigid? Insights from First Principles Calculations

Ido Azuri,[†] Lihi Adler-Abramovich,[‡] Ehud Gazit,[‡] Oded Hod,[§,*] and Leeor Kronik[†,*]

[†]Department of Materials and Interfaces, Weizmann Institute of Science, Rehovoth 76100, Israel

[‡]Department of Molecular Microbiology and Biotechnology, George S. Wise Faculty of Life Sciences, Tel Aviv University, Tel Aviv 69978, Israel

[§]Department of Chemical Physics, School of Chemistry, Raymond and Beverly Sackler Faculty of Exact Sciences, Tel Aviv University, Tel Aviv 69978, Israel

Supporting Information

ABSTRACT: The diphenylalanine peptide self-assembles to form nanotubular structures of remarkable mechanical, piezolelectrical, electrical, and optical properties. The tubes are unexpectedly stiff, with reported Young's moduli of 19−27 GPa that were extracted using two independent techniques. Yet the physical basis for the remarkable rigidity is not fully understood. Here, we calculate the Young's modulus for bulk diphenylalanine peptide from first principles, using density functional theory with dispersive corrections. The calculation demonstrates that at least half of the stiffness of the material is the result of dispersive interactions. We further quantify the nature of various inter- and intramolecular interactions. We reveal that despite the porous nature of the lattice, there is an array of rigid nanotube backbones with interpenetrating "zipper-like" aromatic interlocks that result in stiffness and robustness. This presents a general strategy for the analysis of bioinspired functional materials and may pave the way for rational design of bionanomaterials.

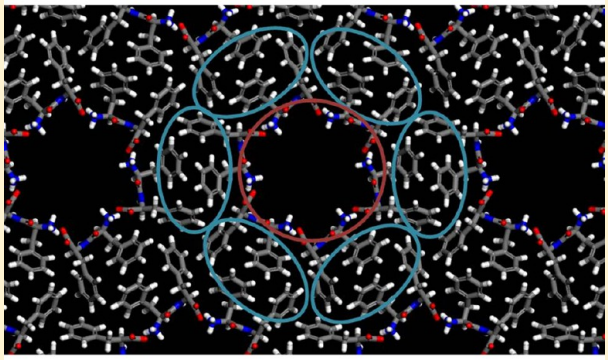

1. INTRODUCTION

Supra-molecular assembly of bioinspired building blocks into well-ordered nanostructures has emerged as a novel route for the development of advanced materials with unique physical and chemical properties.[1,2] One of the most promising building blocks discovered is the aromatic dipeptide, diphenylalanine. Diphenylalanine-based molecular assemblies[3] have been shown to be remarkably physically and chemically stable[4−7] and to possess unique mechanical,[5,7] electrical,[8−10] and optical[8,11] properties. Therefore, they have been at the center of extensive and ongoing scientific attention.[4] One striking property of diphenylalanine-based peptide nanotubes is their remarkable rigidity, as manifested in a reported Young's modulus of 19 GPa, as measured by point stiffness using AFM indentation techniques, followed by finite element analysis.[5] Independent studies using a bending beam model resulted in a Young's modulus of 27 ± 4 GPa.[7] This value is much higher than one might expect for what would traditionally be viewed as a "soft" material and is in fact on par with the Young's modulus of cortical bone.[12,13]

Diphenylalanine is the core recognition motif of the Aβ amyloid polypeptide, which forms fibrilar supra-molecular assemblies in the brain of Alzheimer's disease patients. In fact, amyloid fibrils are found in more than 20 different human disorders and this molecular organization may represent a fundamental low-energy state for polypeptide chains in general.[14,15] The mechanical properties of other fibrils, such as insulin amyloid fibrils were measured and a Young's modulus of 3.3 ± 0.4 GPa was deduced.[16] This mechanical rigidity is quite high in itself and reflects the highly ordered nature of the β-sheet rich amyloid fibrils.[13] Still, the order-of-magnitude higher stiffness of the peptide nanotubes suggests that their ultrastructural features, which ultimately determine their mechanical properties, are not derived from amyloid-like packing alone.

Although well-established experimentally, the molecular origins of this surprising property remain unknown. In the present work, we elucidate the origins of the extreme rigidity found for diphenylalanine-based peptide nanostructures by means of density functional theory (DFT) calculations. Our primary computational vehicle is dispersion-corrected DFT.[17−19] Specifically, we use the Tkatchenko-Scheffler scheme,[17] in which long-range dispersion coefficients and van-der-Waals radii are determined in a parameter-free fashion from the DFT ground state electron density and reference values for the free atoms. Typical approximate exchange-correlation density functionals used in DFT, and in particular

Received: August 22, 2013
Published: December 24, 2013

   dx.doi.org/10.1021/ja408713x | J. Am. Chem. Soc. 2014, 136, 963−969

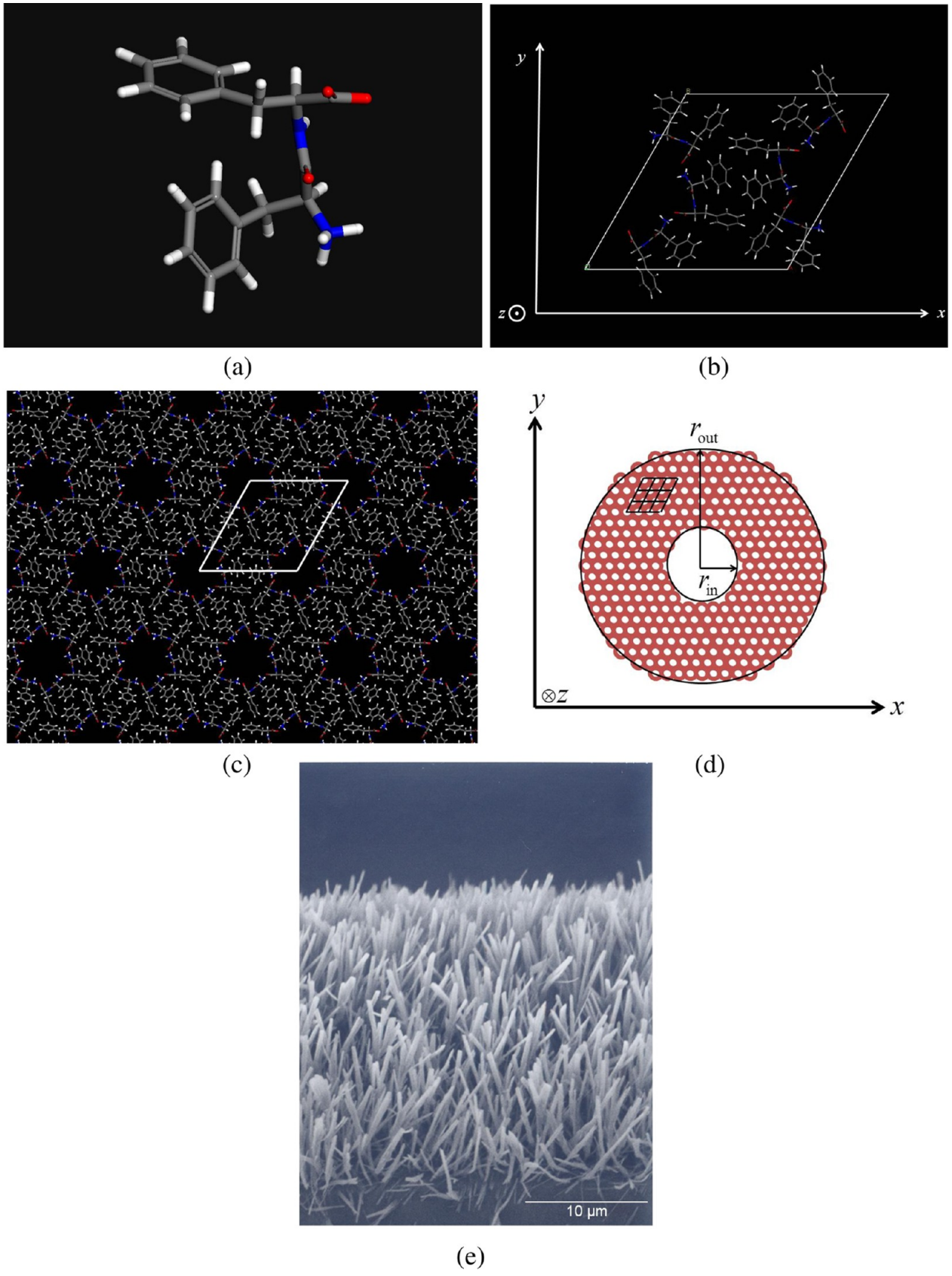

Figure 1. Diphenylalanine-based structures. (a) Diphenylalanine building block, composed of two phenyl side groups attached to the molecular backbone group. (b) Hexagonal unit cell of the diphenylalanine-based molecular crystal, projected onto the *xy* plane. (c) Multiple equivalent unit cells, projected on the *xy* plane, resulting in the characteristic porous molecular crystal structure. The white frame denotes a single unit cell. (d) Schematic illustration of the peptide nanotube structure. (e) Scanning electron microscopy image of a vertically aligned array of diphenylalanine-based structures.

dx.doi.org/10.1021/ja408713x | *J. Am. Chem. Soc.* 2014, 136, 963−969

the nonempirical generalized-gradient approximation of Perdew, Burke, and Ernzerhof (PBE)[20] used below, do very well at describing covalent and ionic bonds. However, they lack the long-range correlation required for the treatment of dispersive interactions. Therefore, they do very poorly in the description of van-der-Waals interaction and possess only limited accuracy in the description of hydrogen bonding. Fortunately, augmenting these approximate functionals with long-range pairwise correction terms, which contain a minimum of adjustable parameters that are fixed once and for all based on benchmark data, enforces the correct asymptotic dispersion interaction between each pair of atoms. This allows for accurate simultaneous treatment of covalent, ionic, hydrogen, and van der Waals bonding, essential for the appropriate description of biomolecular crystals,[21−27] without introducing any system-specific parameters. Here, we use the above-mentioned shortcoming of traditional DFT to our advantage, as comparison of calculations with and without modern dispersive corrections exposes the importance of van der Waals interactions.

By analyzing the separate contribution of different types of chemical interactions, we are able to quantify the specific role of intra- and intermolecular interactions for the overall rigidity of the structure. It is found that despite the porous nature of the crystal structure, unique supra-molecular ordering into an array of rigid nanotube backbones with interpenetrating "zipper-like" aromatic interlocks results in an extremely stiff and robust material.

2. MATERIALS

The peptide diphenylalanine is shown in Figure 1(a). Under suitable conditions, it can form peptide-based nanotubes,[3,5,28] as shown in Figure 1(d, e). The longitudinal direction of the tube is placed along the z axis, whereas in the xy plane, the hollow structure of the tube is revealed with its inner (r_{in}) and outer (r_{out}) radii defined as in Figure 1(d).

In ref 29, it has been shown that both the nanotube and the crystal shapes have the same X-ray structure, which is characterized by a hexagonal unit cell, as shown in Figure 1(b), with the three lattice parameters $|\vec{a}| = |\vec{b}| = 24.071$ Å and $|\vec{c}| = 5.456$ Å. In Figure 1(c), several replicas of equivalent unit cells, forming the bulk material, are shown for clarity. Because the nanotube and the ideal crystal possess the same X-ray structure and because $r_{out} \gg r_{in}$, it is reasonable to assume that the nanotube and the crystal will have similar chemical and physical material properties. Hence, all calculations presented here were performed on the ideal bulk form of the material.

3. GEOMETRY OPTIMIZATION

Crystallographic data were used to construct the unit-cell model of the diphenylalanine molecular crystal.[29] This was followed by full structural relaxation using DFT with and without dispersion corrections (see Computational Details below). The energy of the system, as a function of lattice parameters, was mapped while maintaining the hexagonal symmetry of the unit cell (namely, the angles between the lattice vectors were constrained to $a = \beta = 90°$, $\gamma = 60°$, and the lattice parameters were constrained to fulfill $|\vec{a}| = |\vec{b}|$). Importantly, complete relaxation of all atoms within the unit cell was allowed for any choice of the $\vec{a}$ and $\vec{c}$ lattice vectors. The resulting energy profile, obtained both with and without Tkatchenko-Scheffler dispersive corrections (TS-vdW), is given in Figure 2. The resulting optimized lattice parameters are summarized in Table 1.

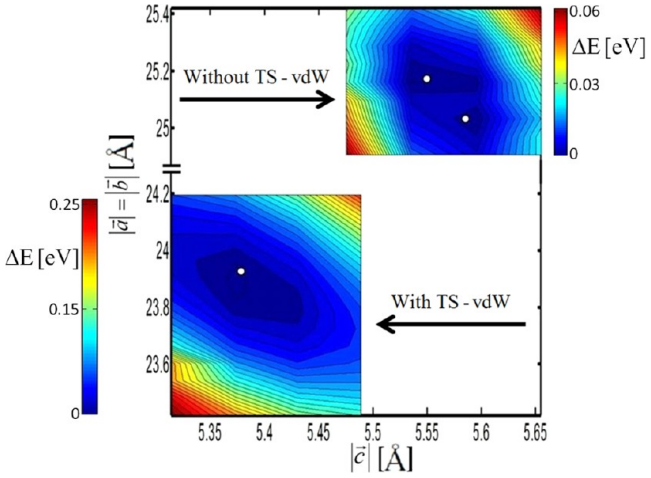

Figure 2. Profile of the energy per unit cell for the diphenylalanine-based hexagonal molecular solid, obtained both with and without Tkatchenko-Scheffler dispersive corrections, as a function of $|\vec{a}| = |\vec{b}|$ and $|\vec{c}|$. White dots indicate energy minima.

It is readily observed that without dispersive corrections, the energy profile contains more than one energy minimum and is more shallow and corrugated. This is because the missing dispersive attraction renders the structure "less physical", as well as less chemically stable, in particular without a very well-defined minimum energy geometrical configuration. Furthermore, as may be expected, in the absence of dispersive interactions the unit cell expands. This behavior is typical for generalized gradient approximation calculations of molecular solids.[21,22] Agreement with the crystallographic data is improved significantly when dispersive corrections are included, bringing it to a level which allows for detailed, quantitative comparison between theory and experiment.[23] We note that for completeness, Table 1 also contains results obtained using an alternative type of dispersive corrections—Grimme's DFT-D2 approach.[18] Both methods improve on the noncorrected results, indicating that this is a general effect. Agreement with experiment is somewhat better with the TS-vdW method. This is likely due to its inherent environment-induced renormalization of the dispersive coefficients. However, we cannot rule out that this improved agreement is fortuitous, as the experimental results may be affected by the presence of water molecules in the molecular crystal pores—an issue not taken into account in our calculations.

4. ELASTIC PROPERTIES

Elastic constants and corresponding Young's moduli can be computed for each of the different computed ground state structures reported in Table 1. Briefly, the calculation proceeds as follows. The strain, α, and the stress, σ, are generally related by the elastic constant tensor, $\mathbf{C}$:[30]

$$\sigma = \mathbf{C}(\alpha - \beta\Delta T) \quad (1)$$

or, equivalently:

$$\alpha = \mathbf{S}\sigma + \beta\Delta T \quad (2)$$

where $\mathbf{S} \equiv \mathbf{C}^{-1}$ is the compliance tensor, β is the thermal expansion coefficient, and ΔT is the temperature change. From

dx.doi.org/10.1021/ja408713x | J. Am. Chem. Soc. 2014, 136, 963−969

Table 1. Experimental and Computed Lattice Parameters (in Å) and Volume (in Å^3), as well as Lattice Parameter Ratio[a]

case	$\|\vec{a}\| = \|\vec{b}\|$	$\|\vec{c}\|$	V_0	$\|\vec{c}\|/\|\vec{a}\|$
crystallographic[b]	24.071	5.456	2737.71	0.226
TS-vdW	23.89 (−0.75%)	5.38 (−1.39%)	2659.16 (−2.87%)	0.225 (−0.44%)
DFT-D2	23.602 (−1.94%)	5.427 (−0.53%)	2618.11 (−4.36%)	0.229 (1.32%)
without vdW[c]	25.062 (4.11%)	5.575 (2.18%)	3032.54 (10.77%)	0.222 (−1.77%)

[a]Numbers in parentheses indicate relative error with respect to experiment. [b]Ref 29 [c]Data correspond to the bottom white dot in Figure 2.

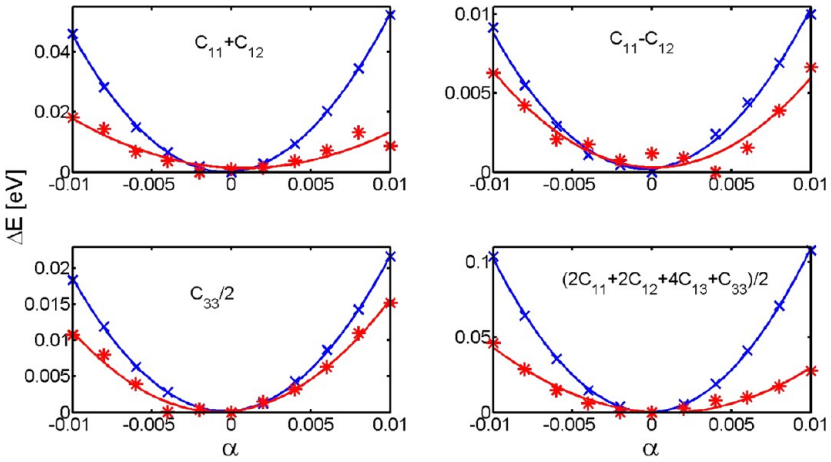

Figure 3. Energy curves, as a function of strain, computed with (blue x signs) and without (red asterisks) TS-vdW corrections, for the following distortions: equal expansion along the x and y directions (top left), equal expansion along the x axis and compression along the y axis (top right), expansion along the z axis (bottom left), and isotropic expansion (bottom right). Solid lines represent a parabolic fit and the elastic constant combination extracted from the curvature of each fit is denoted on each panel.

symmetry considerations, a hexagonal unit cell is characterized by five independent elastic constants,[30,31] given by the following elastic tensor:

$$\mathbf{C} = \begin{pmatrix} C_{11} & C_{12} & C_{13} & 0 & 0 & 0 \\ & C_{11} & C_{13} & 0 & 0 & 0 \\ & & C_{33} & 0 & 0 & 0 \\ & sym & & C_{44} & 0 & 0 \\ & & & & C_{44} & 0 \\ & & & & & (C_{11} - C_{12})/2 \end{pmatrix} \quad (3)$$

The indices in eq 3 are given in the Voigt notation[32] and correspond to the following directions in Cartesian coordinates: $1 \rightarrow xx$, $2 \rightarrow yy$, $3 \rightarrow zz$, $4 \rightarrow yz, xz$. These elastic constants can be calculated from first principles by applying five distinct small distortions to the ground state unit cell. For each of the five distortions, a known combination of elastic constants is extracted from the curvature of the energy versus strain curve, as described in detail in ref 32. The specific distortions required for our calculations, the resulting elastic curves obtained with and without TS-vdW corrections, and the extracted elastic constant combinations are described in Figure 3.

Young's modulus is defined as the ratio between the pressure applied and the resulting deformation, within the elastic limit. Because of the anisotropy of the hexagonal crystal, two distinct Young's moduli can be defined: E_1 in the direction of x or y and E_3 in the direction of z. These Young's moduli can be found from the compliance tensor via the relations $S_{11} = S_{22} = 1/E_1$ and $S_{33} = 1/E_3$.[30,31] Explicitly, this yields:

$$E_1 = (C_{11}^2 C_{33} + 2C_{13}^2 C_{12} - 2C_{13}^2 C_{11} - C_{12}^2 C_{33}) / (C_{11} C_{33} - C_{13}^2) \quad (4a)$$

$$E_3 = (C_{11}^2 C_{33} + 2C_{13}^2 C_{12} - 2C_{13}^2 C_{11} - C_{12}^2 C_{33}) / (C_{11}^2 - C_{12}^2) \quad (4b)$$

The obtained elastic constants, along with the resulting Young's moduli, as well as the Poisson ratio ν_{12} (i.e., minus the ratio of the y and x distortions), are given in Table 2.

Table 2. Elastic Constants (in GPa), Poisson Ratio, and Young's Moduli (in GPa), Computed with and without TS-vdW Dispersive Corrections

case	C_{11}	C_{33}	C_{12}	C_{13}	ν_{12}	E_1	E_3
PBE	5.29	14.08	2.18	2.34	0.36	4.24	12.6
PBE+TS	17.56	24.05	11.91	11.0	0.54[a]	8.75	15.85

[a]The Poisson ratio is theoretically bound: $-1 < \nu < 0.5$. The slight deviation from this bound is attributed to the accumulation of small numerical errors in our computational procedures.

5. DISCUSSION

Two major findings emerge from the data presented in Table 2. First, it is clear that dispersion interactions are indeed essential to the stiffness of the material. In particular, more than half of Young's modulus in the x or y directions is attributed to dispersive interactions. Even in the z direction, where dispersive interactions are not as dominant, Young's modulus still increases by 25% upon their inclusion. Second, the obtained Young's modulus in the x or y directions—~8.8 GPa—is still smaller than the one reported experimentally in ref 5—~19

dx.doi.org/10.1021/ja408713x | J. Am. Chem. Soc. 2014, 136, 963−969

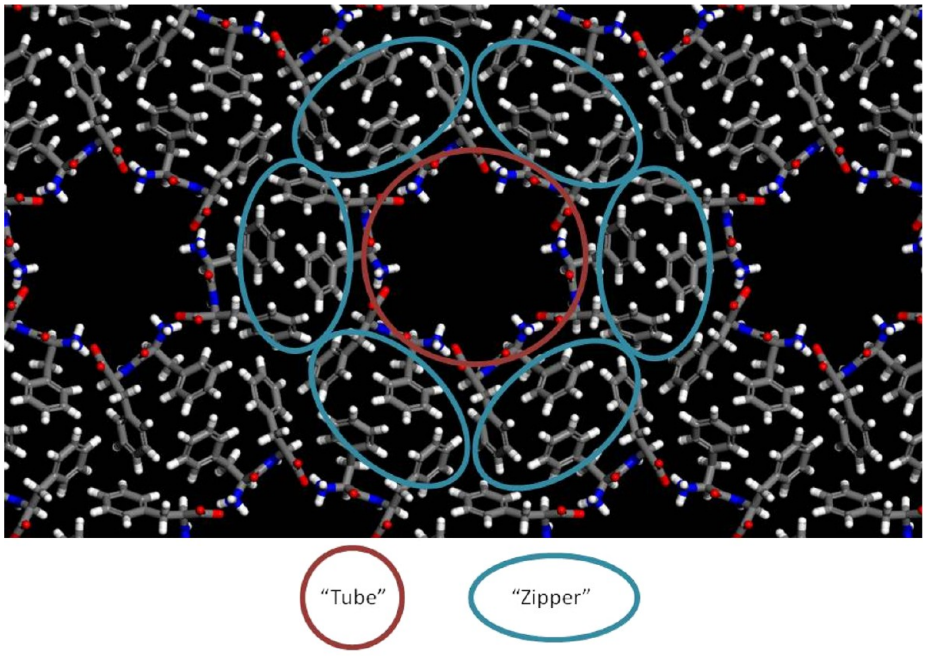

(a)

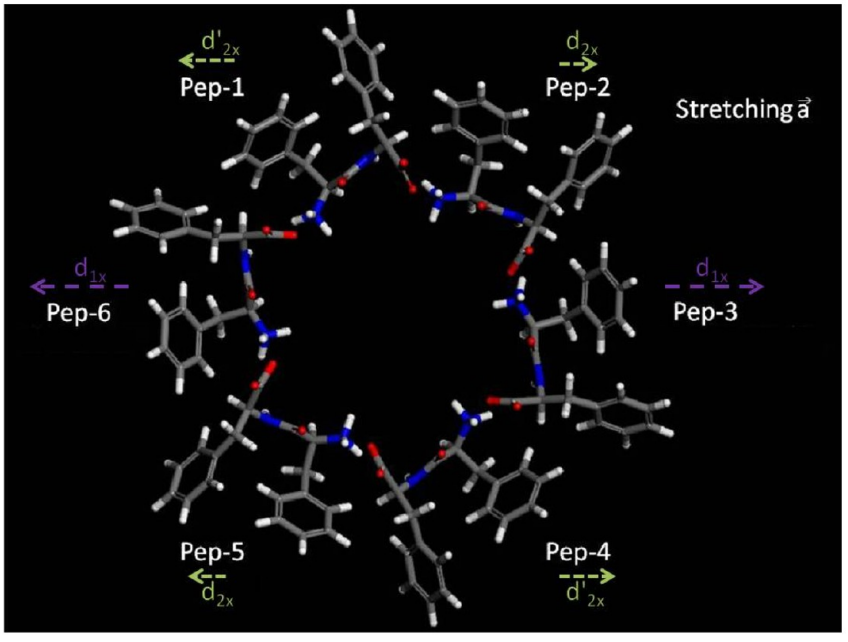

(b)

Figure 4. (a) Schematic partition of the diphenylalanine-based molecular solid into repeating building blocks consisting of an alanine-based "tube" surrounded by six "zipper" units consisting of two diphenyls each. (b) Schematic illustration of center-of-mass movements for each peptide unit upon stretching the *a* lattice parameter along the *x*-direction.

GPa—based on indentation experiments with an atomic force microscope.

Let us address the latter issue first. Obviously, some error can ensue directly from the approximations inherent in our choice of DFT functional and its dispersive corrections. However, given the level of agreement between theory and crystallography, this does not appear to be a plausible explanation for all or even most of the discrepancy. Three other possible differences can be identified. First, as noted above, all simulations were performed on the bulk crystal, whereas all experiments were performed on a peptide tube. Therefore, part of the difference may be simply due to geometrical considerations. Second, the measured value was deduced from a finite element analysis of the raw experimental data. It too relies on certain assumptions, e.g., an isotropic Poisson ratio of 0.3 was used, whereas we determined a higher value associated with the relevant direction, which would have reduced the experimentally determined Young's modulus. Third, while the nanotubes were dehydrated before the mechanical measurements, trapping of residual water molecules

dx.doi.org/10.1021/ja408713x | J. Am. Chem. Soc. 2014, 136, 963−969

inside the pores of the crystalline structure, which may have affected the measured values, cannot be ruled out. Given the uncertainties introduced by each of these three issues, we find the value obtained in our calculations to be sufficiently accurate for gaining further insights.

Having discussed the expected accuracy of our computational results, we turn to analyzing their consequences in terms of structure−function relations. A key observation is that structurally, the molecular crystal can be thought of as possessing a unique supra-molecular ordering, shown in Figure 4(a), in which the structural motif is partitioned into an array of peptide nanotube backbones with six interpenetrating "zipper-like" aromatic interlocks, each consisting of two diphenyls.

Chemically, it is clear that the interaromatic interaction is dominated by van-der-Waals forces. While each individual van-der-Waals interaction is relatively weak, there are many phenyl rings participating in the "zipper-like" structure and so the overall interaction is expected to be significant. The rigidity of the peptide backbone, however, is expected to be highly influenced by interpeptide hydrogen bonding. It is well-known that van-der-Waals interaction is dominated by dispersion and that hydrogen bonding also contains a significant dispersive component. Therefore, rigidity due to either type of bonding is expected to be increased by the inclusion of TS-vdW dispersive corrections, in agreement with our findings.

To establish the relative contribution of the peptide nanotube and the aromatic interlocks to the overall rigidity, we have stretched the lattice vector $\vec{a}$ by 1%, relaxed the atoms within the stretched unit cell, and calculated the displacement of the center of mass of each peptide unit relative to its equilibrium position, as shown in Figure 4(b). We then computed the stretching-induced relative displacement between the two furthest (Pep-3 and Pep-6 in Figure 4(b)) and two closest (Pep-1 and Pep-2 or Pep-4 and Pep-5 in Figure 4 (b)) dipeptides corresponding to the same tube. In the extreme case of an arbitrarily rigid backbone and noninteracting aromatic rings, no stretching-induced relative displacement between the peptide units should be expected, as the peptide nanotubes would merely move apart from each other. In the opposite extreme case of an arbitrarily flexible backbone and an arbitrarily rigid aromatic interlock, the stretching-induced peptide displacement is expected to be 100% of the unit-cell stretching, as all of it should be expressed as an "opening" of the nanotube.

We found that the Pep-3−Pep-6 displacement was 80% of the overall stretch with dispersion corrections, versus 68% without them. For Pep-1−Pep-2, the displacements were 37% and 25% with and without dispersive corrections, respectively. This indicates the crucial role played by the "zipper-like" aromatic interlock, when the stretching is exactly along the interlock axis (Pep-3−Pep-6), the result is much closer to the rigid interlock limit than to the rigid backbone limit, i.e., the distortion associated with opening of the "cage-structure" in the stretched direction dominates over that associated with "opening of the zipper-structure". And because opening the "cage-structure" requires significant energy, overall rigidity of the material is obtained. Even when the stretching is only partially along the interlock axis (Pep-1−Pep-2), the contribution from its rigidity is far from negligible. Furthermore, the fact that the relative contribution of the "zipper" increases in the presence of dispersive corrections is fully consistent with benchmark calculations on the S22 set[33] of weakly interacting complexes.[34] These have shown that the error made by PBE calculations for hydrogen-bonded complexes is not nearly as severe as that made for van-der-Waals bonded complexes and that therefore TS-vdW corrections, although useful for both bonding scenarios, are not nearly as dramatic for hydrogen-bonded systems.

The same logic immediately explains why the stiffness along the z direction is not affected as much. In this direction, the material is more layered, so that the above division into "zipper" and "backbone" contributions does not apply. Clearly, mechanical strength is still aided by dispersive interactions, mostly in the form of $\pi - \pi$ interactions (which also drive the typical "herringbone" structure of organic molecular crystals). However, the interlayer distance is larger than the interpeptide distance in the "zipper region", and the dispersive component is accordingly smaller. This observation is again consistent with our calculations—first, whereas C_{11} increases by more than a factor of 3 upon inclusion of dispersive corrections, C_{33} increases by a more modest factor of 1.7. Second, if one "freezes" C_{33} at its nondispersively corrected value, while including dispersive corrections in all other elastic coefficients, the Young modulus, E_1, still increases significantly relative to its uncorrected value—from ∼4.2 GPa to ∼7.7 GPa. This also explains why "standard" van-der-Waals interactions, e.g., of the herringbone type, are not sufficient to generate outstanding mechanical strength.

The above findings also rationalize the observation, made in the Introduction, that the peptide-based nanotubes share some ultrastructural properties of amyloid fibrils but reveal a remarkably higher elastic modulus. These differences most likely stem from the molecular organization of the amyloid as compared to peptide nanotubes. Whereas the formation of amyloid is generally based on backbone interactions that could be assisted by side-chain interactions, the formation of the nanotubes is consistent with the organization of the aromatic moieties. The contribution of the aromatic "zipper" presented here is unique to the tubes and leads to higher Young modulus values. Future studies, therefore, should be directed toward the design of novel building blocks in which the formation and organization of various types of aromatic-zipper structures could be modulated.

6. COMPUTATIONAL DETAILS

All calculations were performed using the generalized-gradient-approximation (GGA) exchange-correlation functional of Perdew, Burke, and Ernzerhof (PBE),[20] with or without dispersive corrections. In all cases, the Brillouin zone of the crystallographic unit cell was sampled using a Monkhorst-Pack k-grid[35] of $1 \times 1 \times 4$ along the three reciprocal lattice vectors.

All TS-vdW calculations have been performed using FHI-AIMS, an all-electron code with numerical atom-centered basis functions.[36] The calculations have been performed under the "light" setting, including the tier-1 basis functions. Selected calculations for the energy profile and elastic moduli were repeated with the tier-2 basis functions to ascertain convergence, with the mechanical properties affected by less than 2%. All DFT-D2 calculations were performed using VASP, a projector-augmented planewave code.[37] The calculations were performed with an energy planewave cutoff of 725 eV.

■ ASSOCIATED CONTENT

Supporting Information

Total energies (in Hartree) and atomic coordinates for the optimized crystalline structures studied in this work. This material is available free of charge via the Internet at http://pubs.acs.org.

dx.doi.org/10.1021/ja408713x | J. Am. Chem. Soc. 2014, 136, 963−969

AUTHOR INFORMATION

Corresponding Author

odedhod@tau.ac.il; leeor.kronik@weizmann.ac.il

Notes

The authors declare no competing financial interest.

ACKNOWLEDGMENTS

Work at the Weizmann Institute and Tel-Aviv University was supported by the Israel Science Foundation and the Lise Meitner Minerva Center for Computational Chemistry. We thank Alexandre Tkatchenko (Fritz-Haber-Institut, Berlin), Daniel Wagner and Meir Lahav (Weizmann Institute), and Roni Schnek and David Barlam (Ben Gurion University) for helpful discussions, as well as Mark Vilensky and Ariel Biller (Weizmann Institute) for expert technical assistance.

REFERENCES

(1) Aida, T.; Meijer, E. W.; Stupp, S. I. *Science* **2012**, *335*, 813−817.
(2) Reches, M.; Gazit, E. Peptide Nanomaterials: Self-Assembling Peptides as Building Blocks for Novel Materials. In *Nanomaterials Chemistry: Novel Aspects and New Directions*; Rao, C. N. R., Mueller, A., Cheetham, A. K., Eds.; Wiley-VCH: Weinheim, 2007.
(3) Reches, M.; Gazit, E. *Science* **2003**, *300*, 625−627.
(4) Yan, X.; Zhu, P.; Li, J. *Chem. Soc. Rev.* **2010**, *39*, 1877−1890.
(5) Kol, N.; Abramovich, L. A.; Barlam, D.; Shneck, R. Z.; Gazit, E.; Rousso, I. *Nano Lett.* **2005**, *5*, 1343−1346.
(6) Abramovich, L. A.; Reches, M.; Sedman, V. L.; Allen, S.; Tendler, S. J. B.; Gazit, E. *Langmuir* **2006**, *22*, 1313−1320.
(7) Niu, L.; Chen, X.; Allen, S.; Tendler, S. J. B. *Langmuir* **2007**, *23*, 7443−7446.
(8) Hauser, C. A. E.; Zhang, S. *Nature* **2010**, *468*, 516−517.
(9) Kholkin, A.; Amdursky, N.; Bdikin, I.; Gazit, E.; Rosenman, G. *ACS Nano* **2010**, *4*, 610−614.
(10) Bdikin, I.; Bystrov, V.; Kopyl, S.; Lopes, R. P. G.; Delgadillo, I.; Gracio, J.; Mishina, E.; Sigov, A.; Kholkin, A. L. *Appl. Phys. Lett.* **2012**, *100*, 0437021.
(11) Amdursky, N.; Molotskii, M.; Gazit, E.; Rosenman, G. J. *Am. Chem. Soc.* **2010**, *132*, 15632−15636.
(12) Rho, J. Y.; Ashman, R. B.; Turner, C. H. *J. Biomech.* **1993**, *26*, 111−119.
(13) Knowles, T. P. J.; Buehler, M. J. *Nat. Nanotechnol.* **2011**, *6*, 469−479.
(14) Guijarro, J. I.; Sunde, M.; Jones, J. A.; Campbell, I. D.; Dobson, C. M. *Proc. Nat. Acad. Sci. U.S.A.* **1998**, *95*, 4224−4228.
(15) Gazit, E. *Angew. Chem., Int. Ed.* **2002**, *41*, 257−259.
(16) Smith, J. F.; Knowles, T. P. J.; Dobson, C. M.; MacPhee, C. E.; Welland, M. E. *Proc. Natl Acad. Sci. U.S.A.* **2006**, *103*, 15806−15811.
(17) Tkatchenko, A.; Scheffler, M. *Phys. Rev. Lett.* **2009**, *102*, 0730051.
(18) Grimme, S. J. *Comput. Chem.* **2006**, *27*, 1787−1799.
(19) Riley, K. E.; Pitonak, M.; Jurecka, P.; Hobza, P. *Chem. Rev.* **2010**, *110*, 5023−5063.
(20) Perdew, J. P.; Burke, K.; Ernzerhof, M. *Phys. Rev. Lett.* **1996**, *77*, 3865−3868.
(21) Bučko, T.; Hafner, J.; Lebègue, S.; Ángyán, J. G. *J. Phys. Chem. A* **2010**, *114*, 11814−11824.
(22) Al-Saidi, W. A.; Voora, V. K.; Jordan, K. D. J. *Chem. Theor. Comput.* **2012**, *8*, 1503−1513.
(23) Marom, N.; Tkatchenko, A.; Kapishnikov, S.; Kronik, L.; Leiserowitz, L. *Cryst. Growth Des.* **2011**, *11*, 3332−3341.
(24) Graziano, G.; Klimeš, J.; Fernandez-Alonso, F.; Michaelides, A. J. *Phys: Condens. Matter* **2012**, *24*, 4242161−4242168.
(25) Klimeš, J.; Michaelides, A. J. *Chem. Phys.* **2012**, *137*, 1209011−12090112.
(26) Appalakondaiah, S.; Vaitheeswaran, G.; Lebègue, S.; Christensen, N. E.; Svane, A. *Phys. Rev. B* **2012**, *86*, 0351051.
(27) Liu, C. -S.; Pilania, G.; Wang, C.; Ramprasad, R. J. *Phys. Chem. A* **2012**, *116*, 9347−9352.
(28) Abramovich, L. A.; Aronov, D.; Beker, P.; Yevnin, M.; Stempler, S.; Buzhansky, L.; Rosenman, G.; Gazit, E. *Nat. Nanotechnol.* **2009**, *4*, 849−854.
(29) Görbitz, C. H. *Chem. Commun.* **2006**, 2332−2334.
(30) Nye, J. F. *Physical Properties of Crystals: Their Representation by Tensors and Matrices*; Oxford University Press: Oxford, NY, 1957.
(31) Bower, A. F. *Applied Mechanics of Solids*; CRC Press: Boca Raton, FL, 2009.
(32) Fast, L.; Wills, J. M.; Johansson, B.; Eriksson, O. *Phys. Rev. B* **1995**, *51*, 17431−17438.
(33) Jurecka, P.; Sponer, J.; Cerny, J.; Hobza, P. *Phys. Chem. Chem. Phys.* **2006**, *8*, 1985−1993.
(34) Marom, N.; Tkatchenko, A.; Rossi, M.; Gobre, V. V.; Hod, O.; Scheffler, M.; Kronik, L. J. *Chem. Theor. Comput.* **2011**, *7*, 3944−3951.
(35) Monkhorst, H. J.; Pack, J. D. *Phys. Rev. B* **1976**, *13*, 5188−5192.
(36) Blum, V.; Gehrke, R.; Hanke, F.; Havu, P.; Havu, V.; Ren, X.; Reuter, K.; Scheffler, M. *Comput. Phys. Commun.* **2009**, *180*, 2175−2196.
(37) Kresse, G.; Furthmüller, J. J. *Comput. Mater. Sci.* **1996**, *6*, 15−50.